*Desalination and Water Treatment*
www.deswater.com
doi: 10.5004/dwt.2021.27252

226 (2021) 167–176
June

# Preparation and deodorization behavior of copper-modified mesostructured MCM-41 for the treatment of malodorous gas in sewage plants

Fanzhu Meng[a], Fen Li[a,*], Jinguang Hu[b], Cailian Yu[a], Baocai Ge[a]

[a]*Department of Chemistry and Environment Engineering, Harbin University of Science and Technology, Harbin 150040, Heilongjiang, China, emails: hgxylf@126.com (F. Li), 576934131@qq.com (F. Meng), lgyucailian@126.com (C. Yu), 1252791382@qq.com (B. Ge)*
[b]*Department of Chemical and Petroleum Engineering, University of Calgary, Calgary T2N 1N4, Canada, email: jinguang.hu@ucalgary.ca*

Received 9 August 2020; Accepted 14 March 2021

**ABSTRACT**

To find efficient adsorption material for the treatment of malodorous gas in sewage plants, in this study, pure silicon Mobil composition of matter-41 (MCM-41) with cobblestone morphology, a member of the family of mesoporous molecular sieve, was used. Herein, copper-modified MCM-41 (Cu-MCM-41) was prepared by hydrothermal method for $H_2S$ adsorption. The experimental results showed that when the water-to-silicon ratio ($nH_2O$:nTEOS) was 493:1, stirring time was 15 min, and modification amount of copper reached 30%; the $H_2S$ adsorption time on Cu-MCM-41 was close to 90 min and the theoretical sulfur capacity could reach 34 mg $g^{-1}$, which is much higher than the adsorption performance of pure nano-copper oxide. After copper modification, the specific surface area of the sample decreased, and countless small nano CuO particles could be observed in the cobblestone particles. Moreover, these particles were found to be evenly dispersed on the surface and pores of MCM-41, which facilitated the adsorption reaction with $H_2S$, and improved the utilization rate of the active component nano CuO. The adsorbed $H_2S$ mainly existed in the form of CuS, $Cu_2S$, and $CuSO_4$ on the surface of the material, and redox reaction occurred during the adsorption process. This research provides an effective approach for the preparation of new material for the treatment of sulfur-containing malodorous gas.

*Keywords:* MCM-41; Hydrogen sulfide; Deodorization; Copper-modified

## 1. Introduction

In recent years, in order to alleviate the water resource crisis and for partial mitigation of pressure on freshwater resources, a large number of sewage treatment plants have been built; moreover, for achieving this objective, seawater is used for toilet flushing in many cities around the world [1]. When the sulfate content in domestic sewage is too high, the sewage plant produces a large amount of hydrogen sulfide ($H_2S$) odorous gas. Once this type of waste gas diffuses into the atmosphere, it causes serious health hazards to humans. Therefore, the treatment of odorous waste gas in sewage treatment plants remains a critical issue and has become a highly valued problem requiring urgent solutions.

During the investigation, it was found that the currently used treatment methods for odorous waste gas in sewage treatment plants mainly include absorption, adsorption, biological methods, and plasma technologies. However, due to the unsatisfactory deodorization effect of single

* Corresponding author.

treatment technology, combined processes are used more often, which leads to an undesirable increase in the cost of odor treatment. Compared to other deodorization processes, the adsorption method exhibits the characteristics of large adsorption capacity, safe operating conditions, environmental protection, and non-deactivation [2]. Noteworthy, if high-efficiency adsorbent can be developed, the process flow of odor control can be shortened. At present, the most commonly used deodorizing adsorbent in sewage plants is activated carbon (AC). However, owing to the poor deodorization performance of pure AC, it is often modified to improve its adsorption performance [3–6]. For example, Yang et al. [7] prepared a series of N-modified coal-based AC-loaded zinc oxide adsorbents. Xu et al. [8] modified AC with potassium permanganate. Importantly, they all achieved good deodorization effects. However, the pore structure of AC is complex with a wide pore size distribution. As a result, the modification process is likely to cause uneven distribution of deodorizing active components, blockage or destruction of pores, and eventually affecting the further improvement of deodorization performance.

Molecular sieve is a type of hydrated aluminosilicate, a uniform pore structure that has the function of screening molecules. In this study, pure silicon MCM-41 with cobblestone morphology, a member of the family of mesoporous molecular sieve, was used [9,10]. Corporation synthesized MCM-41, an ordered mesoporous material that possesses an excellent porous system. It has attracted significant research attention due to its high specific surface area, high thermal stability, and the possibility of controlling its pore size. These characteristics have made MCM-41 a promising material as a catalyst. It offers a wide range of application prospects in the fields of adsorption, separation, drying and purification, and catalysis. For example, Du et al. [11] and Fu et al. [12] used functional groups to modify MCM-41 to adsorb heavy metal ions such as Hg, Pb(II), and Cd(II). Zhang et al. [13] used graphene combined with MCM-41 to remove tetracycline from water bodies and achieved significant results. Molecular sieves have also been reported as potential candidates for the adsorption of malodorous gases. The H-ZSM-5 type molecular sieve prepared by Hulea et al. [14] and the nickel-modified MCM-41 studied by Ghimire et al. [15] showed high adsorption catalytic performance on mercaptan oxidation. Geng et al. [16] prepared three types of molecular sieves (MCM-41, SBA-15, and MCM-48) loaded with zinc oxide (ZnO) adsorbents. Noteworthy, the adsorbents have large adsorption capacity and can be used through multiple adsorption/regeneration cycles. Khaledyan et al. [17] used iron-modified MCM-41 to obtain a better adsorption effect on the adsorption of $H_2S$ [18]. Wang et al. [19] prepared ZnO-supported SBA-15, which exhibited better $H_2S$ removal effect compared to zinc-modified graphite oxide [20].

The above-mentioned studies indicate that the modified molecular sieve offers a larger adsorption capacity for malodorous gases; however, the modified elements are mostly iron and zinc. The preliminary research by our research group showed that the deodorization performance of nano-CuO is significantly better than that of zinc/iron-based deodorants [21]; nonetheless, there are few reports on copper-modified molecular sieve deodorants. Among the range of molecular sieve materials available, MCM-41 belongs to the mesoporous material with wider pores. The introduction of highly active $H_2S$ adsorbent into the framework of MCM-41 can realize the uniform distribution of active components in the pores and improve the deodorization performance of MCM-41.

In this study, the hydrothermal method was used to *in situ* synthesize copper-modified MCM-41. The performance toward $H_2S$ adsorption was used as the evaluation index. The preparation process conditions of Cu-MCM-41 were optimized through single-factor experiments, and the techniques including X-ray diffraction (XRD), scanning electron microscopy (SEM), transmission electron microscopy (TEM), X-ray photoelectron spectroscopy (XPS), and specific surface area analysis were used to characterize the as-synthesized samples. It is expected that the results of this study may provide new materials for the treatment of odorous gases in wastewater treatment plants. The purpose is to replace inefficient deodorizing materials.

## 2. Experimental

### 2.1. Material preparation

The hydrothermal method was used herein to prepare copper-modified MCM-41 (Cu-MCM-41) [22]. The specific preparation process is as follows: a certain amount of distilled water was taken in a beaker and NaOH was added to adjust the pH to 12.3 ± 0.1. Further, cetyltrimethylammonium bromide (CTAB, 2 g) was added, and after thorough dissolution, the contents were stirred in the water bath at 60°C for 30 min until the solution became clear. The solution was then let sit for 15 min, further, the stirring was continued and tetraethyl orthosilicate (TEOS, 10 mL) was slowly added. When the white flocculent precipitate was produced in the above-mentioned solution, stirring was continued under water bath condition at 60°C, and at the same time, copper nitrate solution (0.5 mol $L^{-1}$) was added dropwise thereto in a certain ratio (when preparing MCM-41, copper nitrate solution is not added in this step). After complete mixing, the solution was stirred for a period and allowed to stand for 15 min. The as-prepared light blue mixture (100 mL) was taken and put into the reaction kettle, which was then placed in an oven at 130°C. Further, the mixture was crystallized for 48 h and the reaction kettle was taken out, the products in the reaction kettle were filtered and washed until neutral, and the solid products were dried in the oven at 80°C for 15 h. The dried product was ground to powder form, placed in a tube muffle furnace for high-temperature calcination, and the tube furnace was heated at a rate of 2°C $min^{-1}$; calcination temperature was 550°C and the holding time was 5.5 h. After calcination, the product was cooled down to room temperature, taken out, and placed in a desiccator, which afforded black Cu-MCM-41 or white MCM-41.

### 2.2. Testing and characterization

#### 2.2.1. Material deodorization performance test

$H_2S$ was used as the adsorbate. The data show that the $H_2S$ concentration of industrial and urban sewage

treatment plants is generally in the range of a few ppm to thousands of ppm [23,24], thus the gas used in this test was a mixture of $H_2S$ and $N_2$ (the concentration of $H_2S$ was 1,000.0 ± 5.0 ppm, China). The test sample (0.0800 ± 0.0005 g) was taken in an absorption tube with an inner diameter of 10 mm. $H_2S$ flow rate was regulated at 20 mL $min^{-1}$. After the flow rate was stable, $H_2S$ was passed into an absorption tube. Aliquots of the sample were taken at the outlet of the absorption tube at certain intervals, and gas chromatography was used to detect the concentration of $H_2S$ in the absorption tube outlet. When the gas concentration exceeded 20.0 ppm, intake was stopped. When the material began to adsorb $H_2S$, the stopwatch was used to judge the material deodorization performance.

#### 2.2.2. Characterization

The $H_2S$ chromatographic analysis was carried out using a GC-9160 gas chromatograph model (Shanghai Ouhua Analytical Instrument Factory, China). The column temperature was 80°C and the inlet temperature was 50°C. Hydrogen flame photometric detector with detecting temperature of 250°C was used and high purity nitrogen (99.999%) was utilized as carrier gas. The external standard method was used to determine the $H_2S$ concentration at the reactor outlet.

XRD analysis was carried out using a D8 advance X-ray diffractometer (Bruker, Germany) with a CuKα radiation source. The tube voltage was 40 kV, the tube current was 40 mA, the scanning range was 5°–80°, and the scanning speed was 2°$min^{-1}$.

SEM analysis was performed using a JSM-6380LV SEM (JEOL Corporation, Japan). The sample was vacuum-filtered and the surface was sprayed with gold before testing.

The morphology and particle size of the material were observed using a Japanese JEX-1200EX TEM, and the test voltage was 80 kV. First, the sample was ultrasonically dispersed with absolute ethanol for 20–30 min, then dropper was used to disperse it on a copper mesh, and then TEM was performed after drying the sample.

The specific surface area and pore structure of the sample were determined using a 3H-2000PS1 instrument (Bethesda Instruments (Beijing) Co., Ltd.). The specific surface analysis range was 0.05 $m^2$ $g^{-1}$, and the pore size analysis range was 3.5–5,000 Å. The specific surface area and pore volume of the sample were calculated by the Brunauer–Emmett–Teller (BET) method and the Barrett–Joyner–Halenda (BJH) method, respectively.

Atomic absorption analysis was carried out using an AA7000 atomic absorption spectrophotometer (Shimadzu Corporation, Japan), with a wavelength range of 190–800 nm, the characteristic concentration of Cu element of ≤0.02 μg $mL^{-1}$, the detection limit of ≤0.005 μg $mL^{-1}$, and RSD of ≤1%.

XPS analysis was carried out using a PHI 5700 ESCA system type X-ray photoelectron spectrophotometer (American Physical Electronics Corporation, America). The X-light source was an Al target, Kα line, 1,486.6 eV voltage irradiated sample excited photoelectron, hemispherical precision electronic energy analyzer, fixed through retarding mode.

## 3. Results and discussion

### 3.1. Optimization of preparation conditions for copper-modified MCM-41

#### 3.1.1. Effect of water-to-silicon ratio on deodorization performance of Cu-MCM-41

The water-to-silicon ratio is an important factor affecting the particle size of MCM-41. Some studies have suggested that the difference in the amount of water during the reaction affects the morphology of the micelles formed by CTAB [25], and ultimately influences the particle size. When the added amount of copper was 40% and the stirring time was 15 min, different materials were obtained by changing the water-silicon ratio ($n_{H_2O}$:$n_{TEOS}$). Fig. 1 exhibits the SEM images of different samples prepared using different water-to-silicon ratios. When the water-to-silicon ratio is 247:1 and 986:1 (Figs. 1a and e), Cu-MCM-41 particles appear to stick to each other, and it is impossible to discriminate the morphology of molecular sieve. It is believed to be caused by the agglomeration of copper oxide on the surface of the material. This can be attributed to the fact that when the amount of water in the reaction system was too small, it affected the precipitation of MCM-41 crystal, and the crystal shape of the obtained crystal was not good; therefore, the copper oxide could not be uniformly dispersed in the pores of MCM-41, resulting in agglomeration. In contrast, when an excessive amount of water was used, the MCM-41 with a smaller particle size was precipitated, thus copper compounds were mostly deposited on the surface of MCM-41 and agglomerated on the surface making the final morphology unclear. When the water-to-silicon ratio was 493:1 (Fig. 1c), Cu-MCM-41 molecular cobblestone exhibited the most complete morphology, the particle size was moderate, and the surface was uniformly dispersed.

Fig. 2 exhibits the time curve of adsorption of $H_2S$ on Cu-MCM-41. The deodorization performance of Cu-MCM-41 is obviously better than that of MCM-41. This is ascribed to the fact that the main component of the MCM-41 molecular sieve is $SiO_2$, and its pores do not have active components that trap odorous gas molecules, and the pores are uniform, mostly through-holes. After $H_2S$ enters the pores, it is difficult to capture, thus the adsorption effect is not ideal. When MCM-41 was modified with copper ions, the high-temperature roasting preparation process causes Cu to be deposited in the form of copper oxide in the pores. Copper oxide offers high adsorption performance for $H_2S$, thus Cu-MCM-41 acquires better deodorization performance.

Fig. 2 further demonstrates that the adsorption of $H_2S$ on MCM-41 and Cu-MCM-41 first increases and then decreases with the increase of water volume. Combined with the surface morphology analysis of Cu-MCM-41, the results indicate that when the water-to-silicon ratio is too high or too low, the Cu-MCM-41 particles are smaller, and the surface agglomeration phenomenon appears. The effective adsorption area of the material is reduced, the utilization rate of the active component copper oxide is reduced, and the deodorization activity is also reduced. When the water-silicon ratio ($n_{H_2O}$:$n_{TEOS}$) is 493:1, Cu-MCM-41 particles are large, with complete morphology, and no

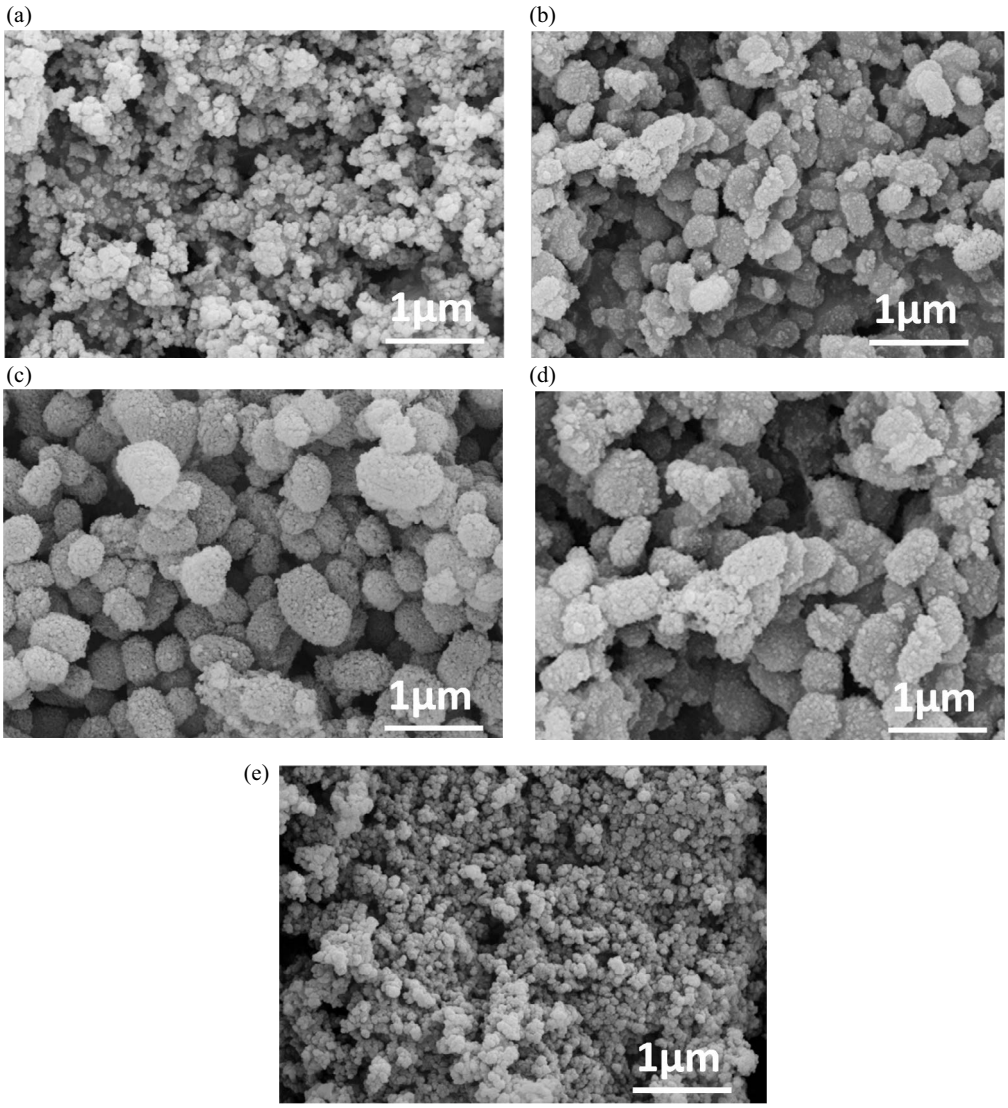


Fig. 1. SEM images of Cu-MCM-41 prepared using different water-to-silicon ratios: (a) 247:1, (b) 370:1, (c) 493:1, (d) 741:1, and (e) 986:1.

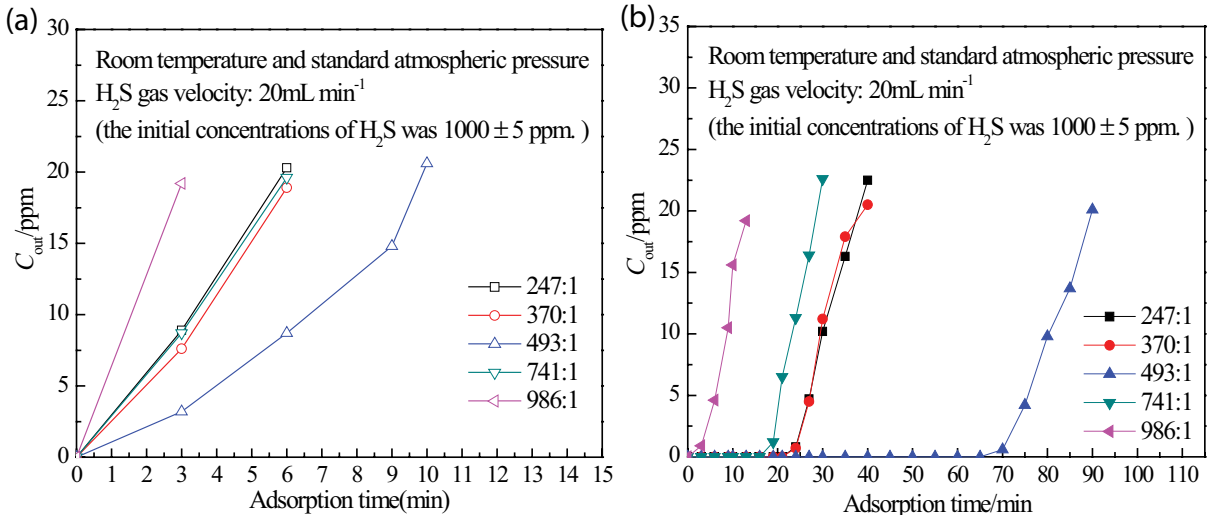


Fig. 2. $H_2S$ adsorption time of MCM-41 and Cu-MCM-41 with different water-to-silicon ratios: (a) MCM-41 and (b) Cu-MCM-41.

agglomeration of active components occurs on the surface, deodorization performance of Cu-MCM-41 is the best, and the adsorption time of $H_2S$ can be close to 90 min.

### 3.1.2. Effect of stirring time on deodorization performance of Cu-MCM-41

Fig. 3 shows the SEM images of MCM-41 and Cu-MCM-41 prepared under different mixing times after mixing all raw materials. Fig. 3a demonstrates that when the stirring time is 5 min, the Cu-MCM-41 particles formed are uneven in size, the edges of the particles are rough, and small particles adhere to the surface. In contrast, when the stirring time is 15 min, the particle morphology is complete, the edges are clear, and some small particles adhere evenly on the surface. For the too long stirring time (Figs. 3c–e), the cobblestone-like morphology of Cu-MCM-41 is broken in a large area to form small particles. The copper oxide loaded on MCM-41 by the co-precipitation reaction falls off and the active components are reduced. Fig. 3e shows that when the stirring reaches 60 min, the surface of the material is almost smooth, and the copper oxide basically falls off from the surface of the material. Combined with the time curve of $H_2S$ adsorption shown in Fig. 4, the results indicate that when the stirring time is extended from 5 to 15 min, the adsorption performance of the sample is slightly improved. The adsorption effect of the Cu-MCM-41 sample is the best when the stirring time is 15 min. However, with the extension of the stirring time, the adsorption performance decreases significantly. It indicates that too long stirring time of the material after mixing is not conducive to the dispersion of the loaded metal on the surface of the material, and the load ratio is reduced, which impacts the adsorption effect. Finally, the

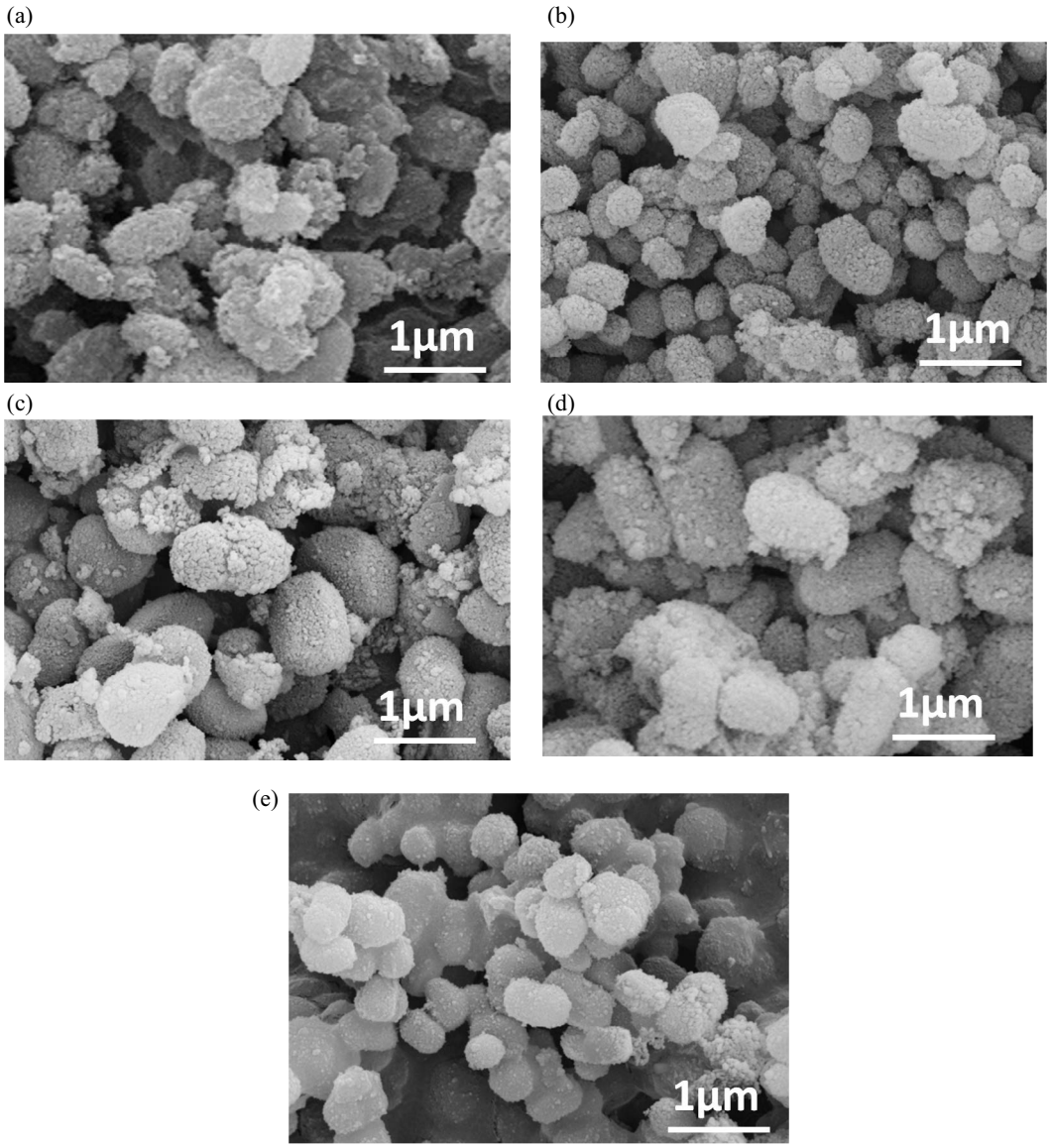


Fig. 3. SEM images of Cu-MCM-41 with different mixing times after mixing all materials: (a) 5 min, (b) 15 min, (c) 30 min, (d) 45 min, and (e) 60 min.

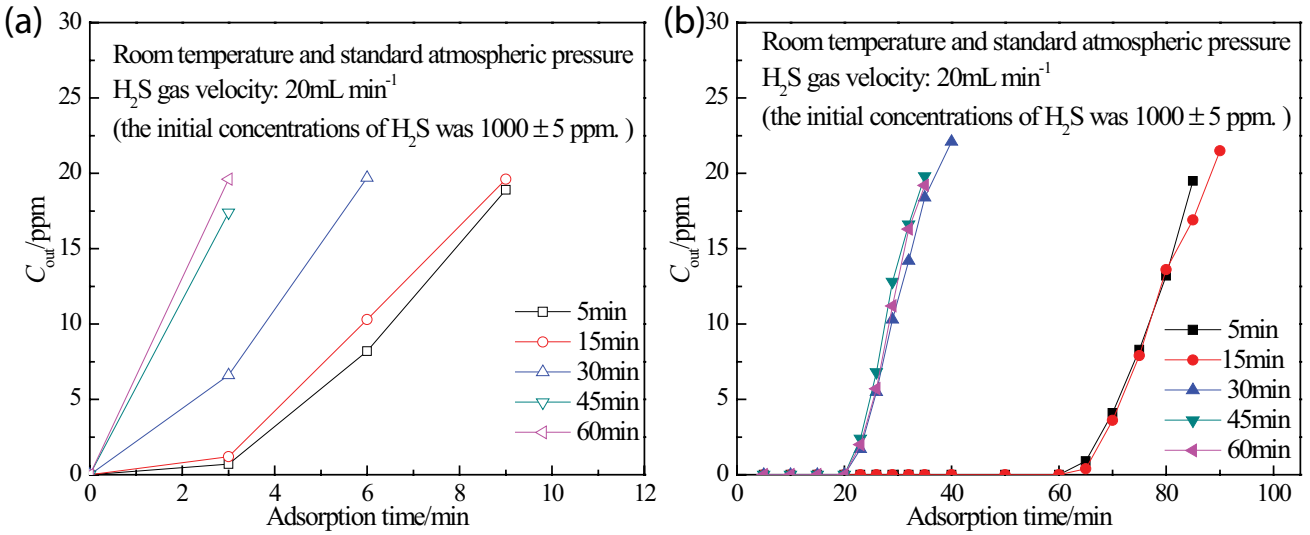


Fig. 4. $H_2S$ adsorption time of MCM-41 and Cu-MCM-41 prepared under different stirring time: (a) MCM-41 and (b) Cu-MCM-41.

optimized stirring time required for the completion of the reaction was determined to be 15 min.

#### *3.1.3. Effect of the amount of copper on the deodorization performance of Cu-MCM-41*

The adsorption effect of MCM-41 for $H_2S$ at room temperature was very poor. The effective adsorption time of MCM-41 (0.0800 g) was about 10 min. Cu co-precipitated with the silicon source during the preparation process of MCM-41. After calcining at high temperature, it could be oxidized to form CuO, which exhibited excellent adsorption performance for $H_2S$. The actual copper load of Cu-MCM-41 was determined by atomic absorption spectrometry. Through experimental investigation, the effect of the amount of copper content on the deodorization performance of Cu-MCM-41 adsorbent was investigated, as shown in Fig. 5. Fig. 5 exhibits that with the increase in the amount of copper, the deodorization time also prolonged. When the copper loading was close to 33.33% and 40.05%, the sample adsorbed $H_2S$ for nearly 90 min. It indicates that copper oxide with a load of about 30.0% on MCM-41 shows a good adsorption effect.

In summary, MCM-41 has poor deodorization activity, while Cu-MCM-41 modified with copper shows significantly improved $H_2S$ adsorption performance. During the preparation process of Cu-MCM-41, when the ratio of water to silicon is 493:1, stirring time is 15 min, and modification amount of copper is 30%; the adsorption performance of the prepared sample becomes optimal. The adsorption time for $H_2S$ is close to 90 min, the theoretical sulfur capacity can reach 34 mg $g^{-1}$, and the deodorization performance is better than or close to those of molecular sieves and carbon-based adsorption materials reported in the literature [26]. The active component of Cu-MCM-41 nano CuO has a theoretical sulfur capacity of up to 113.3 mg $g^{-1}$, which is better than the deodorization performance of nano CuO reported in the literature [21].

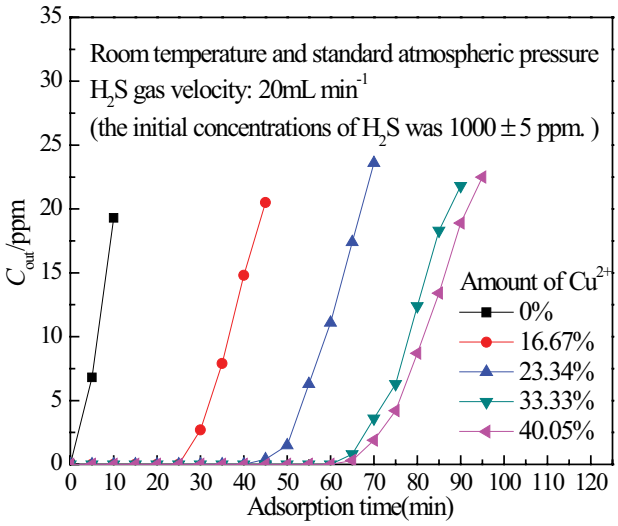


Fig. 5. Cu-MCM-41 adsorption time with different copper loads.

### *3.2. Deodorization structure analysis of Cu-MCM-41*

#### *3.2.1. XRD analysis*

In order to investigate structural characteristics of the molecular sieve adsorbent, molecular sieve modified with copper was characterized by XRD. Fig. 6 shows the characterization results, illustrating that the six-party structure of MCM-41 is still present after copper modification [27], and diffraction peaks appear at 2θ of 2.1°, 3.6°, and 4.2°, which correspond to the PDF standard card, corresponding to the diffraction peaks of the (100), (110), and (200) crystal planes. Further analysis shows that the diffraction peak intensity at 2θ of 35.6° and 38.7°, is relatively large. Compared to the PDF standard card, the diffraction peak at 35.6° is attributed to the CuO($\bar{1}$11) crystal plane, and that at 38.7° is attributed to the CuO(111) crystal plane. With

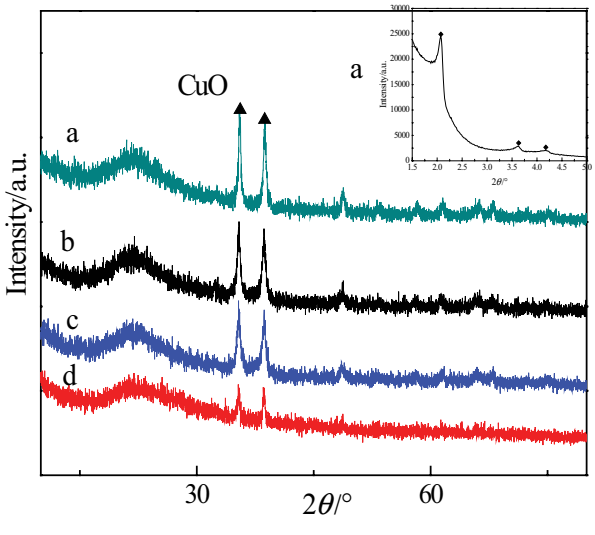


Fig. 6. XRD analysis of Cu-MCM-41 with different copper loads: (a) 40.05%, (b) 33.33%, (c) 23.34%, and (d) 16.67%.

the increase of the amount of modification, the intensity of the diffraction peak is obviously increased. By using the half-width value of the diffraction peaks of the ($\bar{1}11$) and (111) crystal planes, the average grain size of CuO from a to d is 21.2, 14.4,10.8, and 8.6 nm, respectively. It indicates that the grain size of CuO increases with the increase of copper load. Analysis shows that when the load is small, the nano-CuO adheres mostly to the inside of the pores; however, when the load increases, copper oxide particles aggregate on the surface of the sample, and the collision probability of CuO increases, resulting in an increase in the grain size [28]. Analysis of the combined results of adsorption deodorization experiments and electron microscopy analysis indicates that the larger the loading of active component CuO, the better the deodorization. When the loading reaches 33.33%, the deodorization effect is better, CuO size is moderate, and the distribution is uniform.

### 3.2.2. Specific surface area and pore structure analysis

Table 1 lists the specific surface area and pore structure data of the samples. Table 1 summarizes that compared to those of MCM-41, the specific surface area and pore volume of copper-modified samples, that is, Cu-MCM-41, are significantly reduced. However, the proportion of the pore volume of samples with size in the range of 2–50 nm increased significantly, indicating that nano CuO entered the pores of MCM-41, occupied most of the micropores, and got connected to each other on the surface of the material to form a new pore structure. It resulted in the increase in the volume ratio of mesopores and macropores, and the average pore size also increased. However, molecular sieves before and after modification were mainly mesoporous structures. The adsorption effect of MCM-41 before modification was not good, and the adsorption effect after modification was obviously improved, indicating that CuO is the main active component for adsorbing $H_2S$. The specific surface area of Cu-MCM-41 is still relatively large, thus it provides the channel for $H_2S$ to enter the interior of the material, which is beneficial to the adsorption reaction. After Cu-MCM-41 adsorbed $H_2S$, the pore size distribution did not change significantly; however, noteworthy, original macropores disappeared, and specific surface area, average pore size, and pore volume all decreased. This result may be ascribed to the fact that the copper oxide particles trapped gas molecules, and the formed product blocked some pores.

Figs. 7a and b display the nitrogen adsorption and desorption curves before and after the adsorption of $H_2S$ on Cu-MCM-41. Fig. 7a illustrates that according to the IUPAC isotherm type classification, Cu-MCM-41 before adsorption belongs to type III isotherm, and adsorption amount in the low-pressure region is relatively small, about 60 mL $g^{-1}$. The amount of adsorption in the medium pressure zone increases to about 150 mL $g^{-1}$. A large amount of adsorption is observed to occur in high-pressure area; however, comparative analysis of pore structure data presented in Table 1 indicates the accumulation of pores between the MCM-41 molecules and copper oxide particles attached to the surface of MCM-41, resulting in this phenomenon. Fig. 7b shows the nitrogen adsorption and desorption isotherm of Cu-MCM-41 after $H_2S$ adsorption, which still belongs to the type III isotherm, and the total adsorbed amount is about 200 mL $g^{-1}$, which indicates that the deodorization process is likely to generate solid phase products which get fixed in the pores, resulting in a decrease in nitrogen adsorption capacity. The adsorption capacity in the low-pressure region is about 40 mL $g^{-1}$, the adsorption capacity in the mesoporous region is about 60 mL $g^{-1}$, and that in the high-pressure region is about 70 mL $g^{-1}$. Analysis reveals a significant decrease in the amount of mesoporous adsorption, indicating that the reaction mainly takes place in the mesoporous region. Some products are also formed on the surface of Cu-MCM-41; therefore, the accumulated pores with larger pore diameters are occupied with products, and some are converted into micropores or mesopores with smaller pore diameters, and some may be

Table 1
Material specific surface area, pore structure, and pore size distribution data

| Sample | BET ($m^2$ $g^{-1}$) | Pore volume (mL $g^{-1}$) | Average pore size (nm) | Particle size distribution (%) | | |
|---|---|---|---|---|---|---|
| | | | | <2 nm | 2–50 nm | >50 nm |
| MCM-41 | 1,444.0841 | 0.981136 | 2.3771 | 39.3 | 60.6 | 0.1 |
| Cu-MCM-41 | 460.5985 | 0.759710 | 8.0649 | 9.0 | 90.2 | 0.8 |
| Cu-MCM-41 (after adsorbing $H_2S$) | 187.48 | 0.28 | 5.47 | 10.9 | 89.1 | 0.0 |

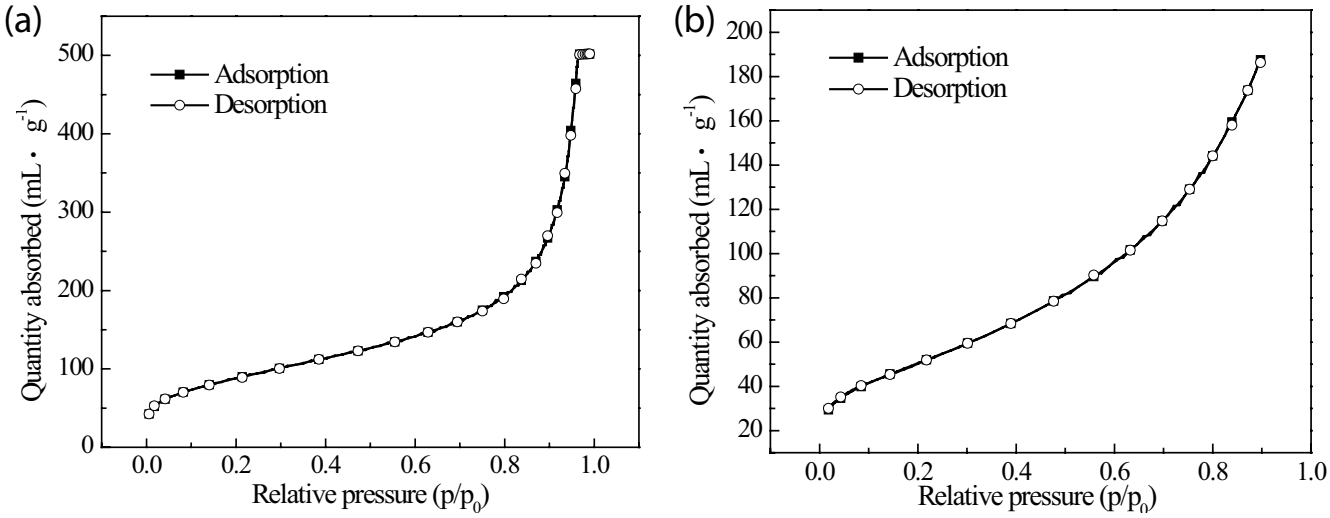


Fig. 7. $N_2$ adsorption/desorption isotherms: (a) Cu-MCM-41 and (b) Cu-MCM-41 after absorbing $H_2S$.

completely occupied by the product directly. Therefore, the adsorption process is mainly concentrated in mesopores.

### 3.2.3. Morphological analysis

The surface morphology of MCM-41 before and after copper modification was characterized by SEM, as shown in Figs. 8a and b. Before modification, the shape of MCM-41 particles is similar to that of pebbles. The surface of the particles is smooth, the particle size distribution is relatively uniform, and the size is about 200 nm. After Cu modification, the surface of the material is rough, and the morphology of MCM-41 cobblestone does not change. A large number of small particles is evenly distributed on the surface of the material. Combined with the results of XRD analysis, it is considered that the smaller particles should be nano-CuO grains. To further analyze the structure of Cu-MCM-41, it was characterized by TEM.

Figs. 8c and d exhibit the TEM images of the samples, revealing that MCM-41 particles are thin around, thick in the middle, and faintly visible stripes are found to appear in the interior, which proves that the pores are formed inside the material. After Cu modification, numerous small CuO particles are visible in cobblestone-like large particles, boundaries between particles are clear, and no residual CuO particles appear near the large particles. It indicates that adhesion between CuO and molecular sieve is strong, and it is uniformly dispersed on the surface of MCM-41 and inside the pores. Combined with the adsorption $H_2S$ test results, this structure facilitates the reaction of $H_2S$ molecules in the pores.

### 3.3. Product analysis of Cu-MCM-41 after $H_2S$ adsorption

Fig. 9a shows the XPS fitting pattern of $Cu_{2p}$ after $H_2S$ adsorption on Cu-MCM-41. The characteristic peaks belonging to $Cu^+$ and $Cu^{2+}$ appear at 932.86 and 933.92 eV, indicating that after $H_2S$ adsorption, Cu in Cu-MCM-41 exists in two forms, $Cu^+$ and $Cu^{2+}$. Fig. 9b shows the XPS fitting pattern of $S_{2p}$ after Cu-MCM-41 adsorbed $H_2S$. Obvious fitting peaks are present at 161.7 and 168.1 eV. Analysis shows that the fitted peak at 161.7 eV belongs to S in CuS and $Cu_2S$. The fitted peak at 168.1 eV belongs to S in $CuSO_4$. It indicates that after $H_2S$ is adsorbed on Cu-MCM-41, S may exist in various valence states, and a complex redox reaction occurs during the chemical adsorption process, resulting in fixing of S on the surface and pores of the adsorbent, achieving the dual purpose of desulfurization and fixing.

## 4. Conclusion

MCM-41 with cobblestone morphology was synthesized by the hydrothermal method. The surface of MCM-41 was found to be smooth, and the specific surface area could reach 1,444.08 $m^2\ g^{-1}$; however, the $H_2S$ adsorption performance was poor. The $H_2S$ adsorption performance of Cu-MCM-41 obtained by modifying MCM-41 with copper was significantly improved. The surface of Cu-MCM-41 was rough. Copper was found to occupy the pores of MCM-41 in the form of nanometer copper oxide and blocked the micropores, thus the specific surface area of Cu-MCM-41 was reduced to 460.60 $m^2\ g^{-1}$. However, evenly distributed nano-CuO particles could be seen on the surface of the material and in the pores, which is conducive to the adsorption of $H_2S$. During the preparation process, different ratios of water to silicon, stirring time, and copper modification amount all affected the particle size of Cu-MCM-41 and the distribution of active component CuO, resulting in changes in the adsorption performance of $H_2S$. When the water-to-silicon ratio of MCM-41 was 493:1, stirring time was 15 min, and modification amount of copper was 33.33%, the prepared Cu-MCM-41 exhibited the longest adsorption time of $H_2S$, nearly 90 min. The utilization rate of nano CuO was significantly improved. A complex redox reaction occurred between $H_2S$ and Cu-MCM-41 during the adsorption process. S was mainly fixed on the surface and pores of Cu-MCM-41 in the form of three compounds, namely, CuS,

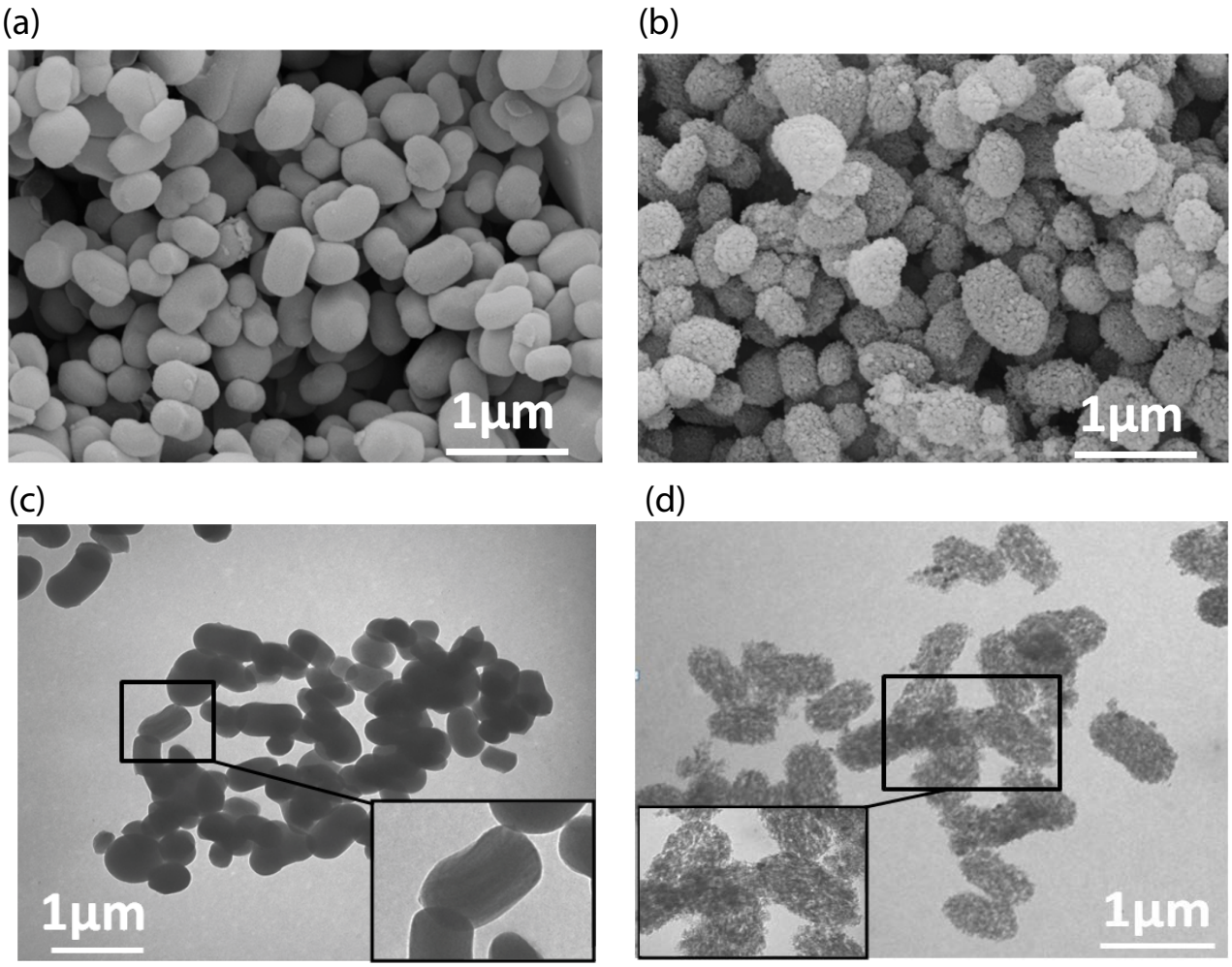


Fig. 8. Electron microscopy images of MCM-41 and Cu-MCM-41: (a) SEM image of MCM-41, (b) SEM image of Cu-MCM-41, (c) TEM image of MCM-41, and (d) TEM image of Cu-MCM-41.

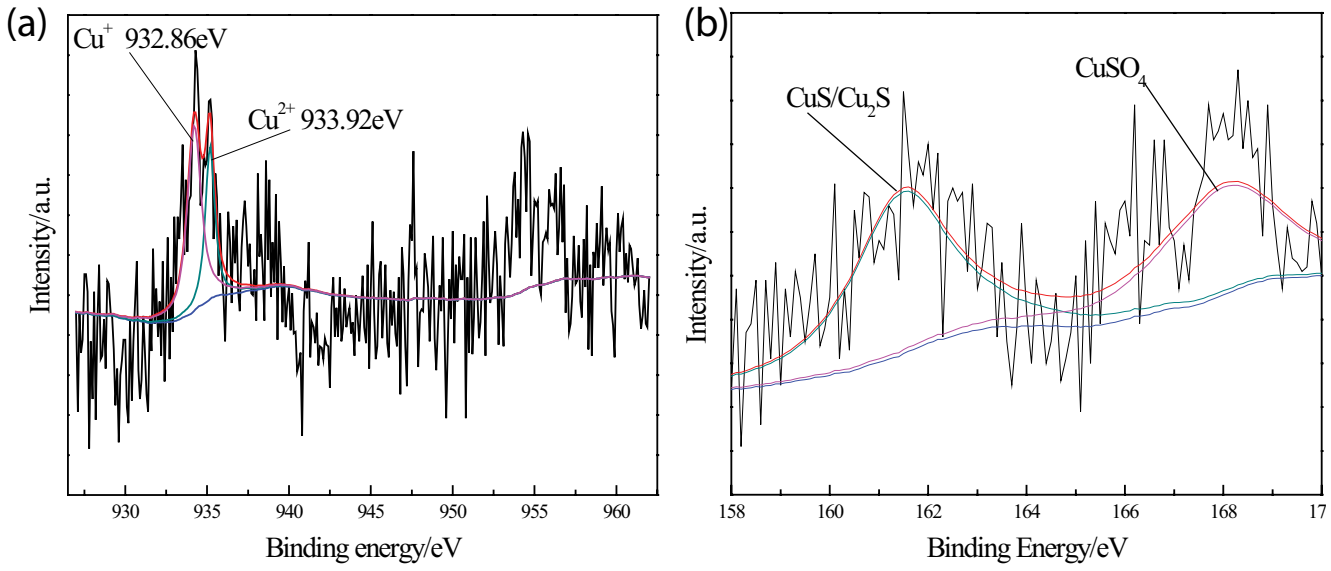


Fig. 9. Fitting spectrum of XPS after adsorption of $H_2S$ on Cu-MCM-41: (a) XPS fitting for $Cu_{2p}$ and (b) XPS fitting for $S_{2p}$.

$Cu_2S$, and $CuSO_4$, resulting in a further decrease in the specific surface area of Cu-MCM-41.

**Acknowledgments**

*Fund project*: National major research and development program (2017YF D0200104).

**Data availability statement**

Some or all data, models, or code that support the findings of this study are available from the corresponding author upon reasonable request.

**References**

[1] S.X. Wang, Y.X. Miao, J.A. Hao, J. Wang, Y.S. Zhang, Analysis on the technological advantages of domestic seawater, Appl. Mech. Mater., 3817 (2015) 692–695.
[2] T. Yu, Y.D. Wang, Z.H. Liu, J.X. Ma, Y. Jing, Recent advances in materials for deep removal of $H_2S$, CIESC J., (2020), doi: 10.11949/0438-1157.20201063.
[3] L. Zhang, A. Hua, L.X. Zhang, The preparation of composite carrier by using diatomite and activated carbon for desulfurization in flue gas, Optoelectron. Adv. Mater. Rapid Commun., 10 (2016) 273–278.
[4] J.A. Arcibar-Orozco, A.A. Acosta-Herrera, J.R. Rangel-Mendez, Simultaneous desulfuration and denitrogenation of model diesel fuel by Fe-Mn microwave modified activated carbon: iron crystalline habit influence on adsorption capacity, J. Cleaner Prod., 218 (2019) 69–82.
[5] Z.R. Liu, J.H. Yu, L.F. Yang, Y. Dai, Y. Wang, L.M. Zhou, Preparation of Fe-loaded activated carbon and its adsorption property of U(VI) in aqueous solution, J. Radioanal. Nuclear Chem., 317 (2018) 1223–1233.
[6] G. De Falco, F. Montagnaro, M. Balsamo, A. Erto, F.A. Deorsola, L. Lisi, S. Cimino, Synergic effect of Zn and Cu oxides dispersed on activated carbon during reactive adsorption of $H_2S$ at room temperature, Microporous Mesoporous Mater., 257 (2018) 135–146.
[7] C. Yang, S. Yang, H.L. Fan, Y.S. Wang, S.G. Ju, Tuning the ZnO-activated carbon interaction through nitrogen modification for enhancing the $H_2S$ removal capacity, J. Colloid Interface Sci., 555 (2019) 548–557.
[8] J.B. Xu, W.Y. Dong, H.J. Wang, X. Huang, Adsorption characteristics of methyl mercaptan in odor by $KMnO_4$ modified activated carbon, Chin. J. Environ. Eng., 14 (2019) 1570–1578.
[9] Q.L. Lu, Y.Q. Li, Advances in hydrothermal synthesis, modification and applications of MCM-41 molecular sieves, Mod. Chem. Ind., 39 (2019) 40–44.
[10] H. Chaudhuri, S. Dash, A.Sarkar, Fabrication of new synthetic routes for functionalised Si-MCM-41 materials as effective adsorbents for water remediation, Ind. Eng. Chem. Res., 55 (2016) 10084–10094.
[11] P.D. Du, N.T. Hieu, T.C. To, G.B. Long, D.Q. Khieu, Aminopropyl functionalised MCM-41: synthesis and application for adsorption of Pb(II) and Cd(II), Adv. Mater. Sci. Eng., 2019 (2019) 1–15, doi: 10.1155/2019/8573451.
[12] Y. Fu, Y. Huang, J.S. Hu, Preparation of chitosan/MCM-41-PAA nanocomposites and the adsorption behaviour of Hg(II) ions, R. Soc. Open Sci., 5 (2018) 171927, doi: 10.1098/rsos.171927.
[13] B. Zhang, T. Wu, D.J. Sun, $NH_2$-MCM-41 supported on nitrogen-doped graphene as bifunctional composites for removing phenol compounds: synergistic effect between catalytic degradation and adsorption, Carbon, 147 (2019) 312–322.
[14] V. Hulea, E. Huguet, C. Cammarano, A. Lacarriere, R. Durand, C. Leroi, R. Cadours, B. Coq, Conversion of methyl mercaptan and methanol to hydrocarbons over solid acid catalysts - a comparative study, Appl. Catal., B, 144 (2014) 547–553.
[15] P. Ghimire, L.P. Zhang, U.A. Kinga, Q.Y. Guo, Development of nickel-incorporated MCM-41-carbon composites and their application in nitrophenol reduction, J. Mater. Chem. A, 7 (2019) 9618–9628.
[16] Q. Geng, L.J. Wang, C. Yang, H.Y. Zhang, Y.R. Zhao, H.L. Fan, C. Huo, Room-temperature hydrogen sulfide removal with zinc oxide nanoparticle/molecular sieve prepared by melt infiltration, Fuel Process. Technol., 185 (2019) 26–37.
[17] E. Khaledyan, K. Alizadeh, Y. Mansourpanah, Synthesis of magnetic nanocomposite core–shell $Fe_3O_4$@MCM-41-$NH_2$ and its application for removal of congo red from aqueous solutions, Iran. J. Sci. Technol. Trans. A Sci., 43 (2019) 801–811.
[18] C. Cara, E. Rombi, A. Ardu, Sub-micrometric MCM-41 particles as support to design efficient and regenerable maghemite-based sorbent for $H_2S$ removal, J. Nanosci. Nanotechnol., 19 (2019) 5035–5042.
[19] X.H. Wang, T.H. Sun, J. Yang, L. Zhao, J.P. Jia, Low-temperature $H_2S$ removal from gas streams with SBA-15 supported ZnO nanoparticles, Chem. Eng. J., 142 (2008) 48–55.
[20] H.S. Song, M.G. Park, S.J. Kwon, K.B. Yi, E. Croiset, Z.W. Chen, S.C. Nam, Hydrogen sulfide adsorption on nano-sized zinc oxide/reduced graphite oxide composite at ambient condition, Appl. Surf. Sci., 276 (2013) 646–652.
[21] F. Li, T. Lei, Y. Yang, Y.P. Zhang, G.H. Yang, Preparation of nano-CuO and its removal performance of $H_2S$ at room temperature, J. Mater. Eng., 43 (2015) 1–6.
[22] X. Hong, K. Tang, Preparation and adsorption denitrification of heteroatoms mesoporous molecular sieve Co-MCM-41, J. Fuel Chem. Technol., 43 (2015) 720–727.
[23] B.W. Yan, Quantitative Relation Study of Odorous Pollutants Based on Sensory Measurement and GC/MS, Harbin Institute of Technology, 2019.
[24] C.M. Liu, H. Dou, J.B. Jiang, Y. Gao, W.Q. Zhang, Study on waste gas emission characteristics and treatment effect of sewage treatment process of a pharmaceutical enterprise in Shijiazhuang City, Hebei J. Ind. Sci. Technol., 35 (2018) 363–369.
[25] J.M. Zhang, J. Liu, H.J. Li, G.P. Wang, $H_2O$/Si ratio action in MCM-41 molecular sieve synthesis and MB adsorption capability, Ind. Water Treat., 38 (2018) 73–76.
[26] A. Peluso, N. Gargiulo, P. Aprea, F.P.D. Caputo, Nanoporous materials as $H_2S$ adsorbents for biogas purification: a review, Sep. Purif. Rev., 48 (2019) 79–89.
[27] K. Sehaspreet, P. Jai, K. Vikas, Single and binary adsorption of Zn(II) and Cr(VI) heavy metals onto synthesized silica-based MCM-41, Chemistry Select, 4 (2019) 2576–2584.
[28] F. Li, Y.P. Zhang, Y. Yang, J. Wei, B. Yan, Structure of activated carbon supported with nano-ZnO and its removal performance of $H_2S$ at room temperature, J. Chin. Ceram. Soc., 40 (2012) 800–805.